Journal of Sound and Vibration 384 (2016) 177–193

Contents lists available at ScienceDirect

Journal of Sound and Vibration

journal homepage: www.elsevier.com/locate/jsvi

A one dimensional numerical approach for computing the eigenmodes of elastic waves in buried pipelines

Wenbo Duan [a,*], Ray Kirby [a], Peter Mudge [b], Tat-Hean Gan [a,b]

[a] Department of Mechanical, Aerospace and Civil Engineering, Brunel University London, Uxbridge, Middlesex UB8 3PH, UK
[b] Integrity Management Group, TWI Ltd, Cambridge CB21 6AL, UK

ARTICLE INFO

Article history:
Received 21 December 2015
Received in revised form
4 May 2016
Accepted 8 August 2016
Handling Editor: G. Degrande
Available online 21 August 2016

Keywords:
Dispersion curves
Coated and buried pipes
One dimensional PML
SAFE method
Exponential coordinate stretching function

ABSTRACT

Ultrasonic guided waves are often used in the detection of defects in oil and gas pipelines. It is common for these pipelines to be buried underground and this may restrict the length of the pipe that can be successfully tested. This is because acoustic energy travelling along the pipe walls may radiate out into the surrounding medium. Accordingly, it is important to develop a better understanding of the way in which elastic waves propagate along the walls of buried pipes, and so in this article a numerical model is developed that is suitable for computing the eigenmodes for uncoated and coated buried pipes. This is achieved by combining a one dimensional eigensolution based on the semi-analytic finite element (SAFE) method, with a perfectly matched layer (PML) for the infinite medium surrounding the pipe. This article also explores an alternative exponential complex coordinate stretching function for the PML in order to improve solution convergence. It is shown for buried pipelines that accurate solutions may be obtained over the entire frequency range typically used in long range ultrasonic testing (LRUT) using a PML layer with a thickness equal to the pipe wall thickness. This delivers a fast and computationally efficient method and it is shown for pipes buried in sand or soil that relevant eigenmodes can be computed and sorted in less than one second using relatively modest computer hardware. The method is also used to find eigenmodes for a buried pipe coated with the viscoelastic material bitumen. It was recently observed in the literature that a viscoelastic coating may effectively isolate particular eigenmodes so that energy does not radiate from these modes into the surrounding [elastic] medium. A similar effect is also observed in this article and it is shown that this occurs even for a relatively thin layer of bitumen, and when the shear impedance of the coating material is larger than that of the surrounding medium.

1. Introduction

It is common to locate defects or ruptures in pipelines by monitoring the propagation of acoustic energy travelling along the walls of the pipe. For example, in non-destructive testing an ultrasonic guided wave is used to interrogate the structural integrity of the pipeline [1,2], whereas at much lower [audio] frequencies one may detect propagating elastic waves generated by pipe ruptures [3,4]. These techniques are well developed and they generally work well for pipeline applications

* Corresponding author.
E-mail address: wenbo.duan@brunel.ac.uk (W. Duan).

http://dx.doi.org/10.1016/j.jsv.2016.08.013
0022-460X/

where the attenuation of the propagating wave is negligible. However, in many pipeline applications it is common for some form of attenuation to be present. For example, viscoelastic coatings are often present and they attenuate energy as the wave travels along the pipe wall. This limits the inspection range of non-destructive techniques such as long range ultrasonic testing [5–7]. Furthermore, pipelines are often buried underground and acoustic energy radiates out from the pipe so that the energy remaining in the pipe wall is reduced [4]. This means that it is potentially more difficult to use pulse-echo based techniques to locate defects and ruptures in pipes that are buried and/or coated. Accordingly, this article presents a fast numerical method suitable for obtaining the eigenmodes for a buried pipe, which may then be used to optimise detection techniques.

In long range ultrasonic testing, acoustic energy is generated using transducers attached around the circumference of a pipe. If one assumes that the pipeline of interest is long and slender then the acoustic energy travels along the pipe walls in a discrete set of pipe eigenmodes. Knowledge of the properties of these eigenmodes is essential in order to fully interpret information obtained from a testing regime. A popular approach for obtaining these eigenmodes is through the solution of an analytic expression for the governing dispersion relation. For example, Lowe et al. [8,9] show that by adopting a general matrix method it is possible to obtain eigenmodes for multiple layers, which enables the addition of viscoelastic coatings and/or a surrounding elastic medium such as that encountered by buried pipes [10–12]. Analytic techniques have also been used to study the signals generated by pipe ruptures, for example Muggleton et al. [4] obtained the axisymmetric modes for a buried fluid-filled plastic pipe. The use of analytic techniques to find guided wave properties in buried or embedded structures does however present a number of challenges, and these are mostly associated with finding the roots of an analytic dispersion relation. When one adds complexity to the problem, such as through the addition of a coating and/or a surrounding elastic medium, then root finding becomes ever more problematic. This is because it becomes much harder to track and locate roots in the complex plane and one needs to develop sophisticated algorithms to do this over multiple frequencies. Furthermore, if one wishes to find a large number of eigenmodes then the difficulties with root finding multiply, and it is common to miss modes when attempting to track large numbers of roots through the complex plane. This means that for problems in which complex roots are present, and where one would like to locate a significant number of these roots, root finding can become time consuming and difficult to automate [13]. It is, therefore, not surprising to see that those modes obtained following the solution of an analytic dispersion relation are generally restricted to lower order/axisymmetric modes. For instance, Leinov et al. examine T(0,1) and L(0,2) [12], whereas for imbedded bars Pavlakovic et al. [14] restrict their analysis to [axisymmetric] longitudinal modes and the first flexural mode. Simmons et al. [15] also used an analytic expression to obtain axisymmetric modes for buried bars, or rods, and showed how the argument principle may be used to aid in root finding.

If one wishes to avoid root finding then it is necessary to move towards numerical methods. Whilst this change of approach may be desirable for the analysis of coated pipes and/or more complex multi-layered problems, one may argue that numerical methods are unavoidable when large numbers of eigenmodes are required for use in techniques developed for wave scattering problems [2,16]. A number of different numerical methods are available for finding the eigenmodes for pipes; however, the authors favour the so-called semi-analytic finite element (SAFE) method as it is computationally efficient and it may readily be applied to pipelines with multiple layers, see for example Marzani et al. [17], and for coated pipes see refs. [5–7], as well as Mu and Rose [18]. The extension of the SAFE method to problems involving structures embedded in an infinite medium is, however, less straightforward. The SAFE method requires the solution domain to be closed, which presents a problem for pipes buried in a nominally infinite, or open, medium. This problem was first addressed by Castaings and Lowe [19], who studied a steel rod surrounded by concrete. Castaings and Lowe used a finite element discretisation for the steel rod, and a concentric portion of the surrounding concrete, they then closed the problem with an outer absorbing layer designed to prevent erroneous reflections from the [artificial] boundary of the problem. Castaings and Lowe successfully obtained low order longitudinal and flexural modes, although the accuracy of the method depends on the success of their absorbing layer. Here, Castaings and Lowe note problems with the ability of the layer to absorb longer wavelengths, which was seen in inaccuracies found with the computation of leaky modes with high radiation angles, as well as those modes found at lower ultrasonic frequencies. Moreover, even away from these limiting cases it was found to be necessary to extend the outer boundary of the problem to 16 times the radius of the rod. Thus, the method requires the use of a large number of degrees of freedom, even for a relatively thin rod, and so the absorbing layer proposed by Castaings and Lowe is unlikely to be computationally efficient for problems involving much larger pipework.

An alternative to the use of an absorbing layer was later proposed by Hua et al. [20], who replaced this layer with infinite elements. Hua et al. analysed coated and uncoated pipes buried in soil and they obtained a large number of axisymmetric and flexural modes. The infinite elements used by Hua et al. are popular in the solution of the Helmholtz Equation because they have the potential to be more computationally efficient than absorbing layers. The application of infinite elements requires the discretisation of the exterior domain using elements with an asymptotic or wave based shape function so that one may properly enforce the appropriate radiation boundary condition. However, in regions of high modal scattering it is necessary to increase the radial order of the infinite elements in order to maintain solution accuracy; moreover, infinite elements are also known to suffer from problems with numerical instabilities [21].

Alternative numerical methods for analysing embedded waveguides include a Scaled Boundary Finite Element Method (SBFEM) proposed by Gravenkamp et al. [22,23]. Gravenkamp et al. used the SBFEM in the same way that previous authors had applied the SAFE method, but this time they closed the problem using a numerical dashpot, which was chosen to simulate the appropriate boundary condition. Gravenkamp et al. successfully applied this method to axisymmetric problems

using a one dimensional SBFEM formulation, as well as non-axisymmetric problems using a two dimensional formulation. The dashpot used by Gravenkamp et al. is, however, only an approximation of the appropriate boundary condition between the waveguide and the surrounding medium. This may lead to inaccuracies when, for example, there is a high impedance mismatch between the two regions. An alternative method for closing the problem was presented by Mazzotti et al. [24], who proposed a SAFE based formulation closed by a 2.5D Boundary Element formulation. This method was applied in the analysis of non-axisymmetric embedded waveguides, where the use of boundary elements ensures that the appropriate radiation condition is properly enforced over the surface of the SAFE region. However, the addition of the 2.5D boundary element formulation does present a number of numerical challenges, which may be avoided by using alternative formulations if one is only interested in axisymmetric problems.

A popular alternative for closing numerical models for infinite domains is to use a perfectly matched layer (PML). This method was first introduced by Berenger [25] in the analysis of electromagnetic waveguides and it has become increasingly popular due to the relatively straightforward way in which the method can be integrated into existing finite element based software [26,27]. For this reason, PMLs are widely used in the study of wave propagation and they form the basis of most commercial FE based software. Moreover, a PML is capable of attenuating the outgoing wave much more efficiently than an equivalent absorbing layer such as the one used by Castaings and Lowe [19]. However, it is only recently that a PML has been applied in the analysis of buried pipes. This was accomplished by Nguyen et al. [28], who used the SAFE method to discretise an elastic waveguide of arbitrary cross-section, and then closed the problem using either a rectangular or circular PML layer. Nguyen et al. go on to present a large number of eigenmodes for a steel bar embedded in concrete, as well as a steel rod embedded in stiff stone and a square steel rod embedded in grout. It is demonstrated by Nguyen et al. that the problem may be solved with a PML that has the same thickness as the radius of their waveguide, which shows a significant improvement on the [much larger] absorbing layer used by Castaings and Lowe [19].

The SAFE-PML method presented by Nguyen et al. [28] demonstrates that it is possible to use a numerically based method to recover a large number of eigenmodes for a buried waveguide. However, their method adopts a two-dimensional discretisation of the problem and this generates large numbers of radiation eigenmodes, most of which are of little physical interest. Moreover, the PML layer generates its own [radiation] eigenmodes and these must also be removed when filtering the unordered list of eigenvalues obtained on solution of the problem. Accordingly, it is not uncommon to obtain hundreds of additional radiation modes for each low order non-radiating mode required for the buried waveguide. This means that when using a two dimensional approach, large numbers of degrees of freedom are still required in order to obtain accurate predictions for a relatively small number of non-radiating eigenmodes. The models presented by Castaings and Lowe [19], and Nguyen et al. [28] are, of course, two dimensional models in order to permit the analysis of non-axisymmetric waveguides. However, buried pipelines are likely to represent a large majority of the applications for long range ultrasonic testing, and this means it is necessary to analyse structures larger than those studied by Nguyen et al. This places significant demands on the computational efficiency of a 2D numerical model and it is desirable to develop efficient alternatives if one is to successfully analyse pipelines with dimensions typically found in the field. One way of doing this is to dedicate the analysis to axisymmetric geometries and to take advantage of symmetry.

Accordingly, in this article we return to a one dimensional formulation of the SAFE method similar to that proposed by Hua et al. [20], and Gravenkamp et al. [22,23]. However, rather than using infinite elements [20], or a numerical dashpot [22], to close the one dimensional problem this article uses a PML. In order to do this, it is necessary first to return to a more general Galerkin based writing of the SAFE equations, which then facilitates the addition of a one dimensional PML. Furthermore, a new one dimensional PML stretching function is also investigated with the aim of further reducing the degrees of freedom required for a buried pipe and hence optimising solution time. Accordingly, in Section 2 of this article the governing equations are presented for an axisymmetric embedded waveguide using a one-dimensional SAFE-PML formulation. In Section 3, an exponential PML coordinate stretching function is introduced and predictions are benchmarked against those of Castaings and Lowe [19], Nguyen et al. [28] and DISPERSE [9]. In Section 4, the method is applied to pipelines with geometries typically found in the field, and this focusses on the addition of a viscoelastic coating and investigates recent observations by Leinov et al. [12]. Finally, conclusions are presented in Section 5.

2. Theory

The analysis in this article is restricted to axisymmetric geometries, however it is written in a general form in order to accommodate an arbitrary number of layers that may include, for example, viscoelastic coatings. The pipe substrate is numbered $j=1$, and additional layers are numbered $j=2$ to $m-1$; the outer PML layer is numbered $j=m$, see Fig. 1.

2.1. Governing equations

The governing wave equation for layer j is given by Navier's equation, which in cylindrical coordinates yields [29]

$$\rho_j \frac{\partial^2 u'_{r_j}}{\partial t^2} = \frac{\partial \sigma'_{rr_j}}{\partial r} + \frac{1}{r}\frac{\partial \sigma'_{r\theta_j}}{\partial \theta} + \frac{\partial \sigma'_{rz_j}}{\partial z} + \frac{1}{r}\left(\sigma'_{rr_j} - \sigma'_{\theta\theta_j}\right), \tag{1a}$$

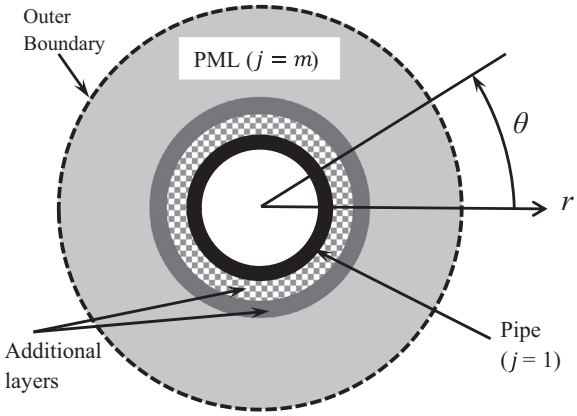

Fig. 1. Geometry of buried pipe surrounded by multiple layers.

$$\rho_j \frac{\partial^2 u'_{\theta_j}}{\partial t^2} = \frac{\partial \sigma'_{\theta r_j}}{\partial r} + \frac{1}{r}\frac{\partial \sigma'_{\theta\theta_j}}{\partial \theta} + \frac{\partial \sigma'_{\theta z_j}}{\partial z} + \frac{2}{r}\sigma'_{r\theta_j}, \tag{1b}$$

$$\rho_j \frac{\partial^2 u'_{z_j}}{\partial t^2} = \frac{\partial \sigma'_{z r_j}}{\partial r} + \frac{1}{r}\frac{\partial \sigma'_{z\theta_j}}{\partial \theta} + \frac{\partial \sigma'_{z z_j}}{\partial z} + \frac{1}{r}\sigma'_{rz_j}, \tag{1c}$$

where r, θ and z form an orthogonal cylindrical coordinate system in the radial, circumferential and axial direction of the waveguide, respectively, ρ is density, t is time, u'_q ($q = r, \theta$ or z) is the displacement in the q direction, and σ'_{ql} ($q, l = r, \theta$ or z) is a symmetric stress tensor of rank two. A time dependence of $e^{i\omega t}$ is assumed throughout this article, where ω is the radian frequency and $i = \sqrt{-1}$. Each layer is assumed to be homogenous and isotropic, and so the usual relationships between stresses and strains hold [29]. To obtain a one dimensional eigensolution the usual ansatz is applied, so that the displacement sound field is assumed to be harmonic in the circumferential direction, and the coupled displacement u'_q for all layers is expanded in the form

$$u'_q(r, \theta, z) = u_q(r) e^{i(-n\theta - k\gamma z)}, q = r, \theta \text{ or } z, \tag{2}$$

where u_q is an eigenfunction, and γ is a dimensionless wavenumber. In addition, n denotes circumferential mode order, $k = \omega/c_T$, and c_T and c_L are the shear (torsional) and compressional (longitudinal) bulk wave velocities of the waveguide, respectively.

A Galerkin based derivation of the SAFE method proceeds by weighting Eq. (1) using the function w_q. The weak forms of Eq. (1) are then obtained by making use of the usual relationships between stress and strain [29] and substituting Eq. (2) into Eq. (1). Following integration by parts in the radial direction the governing equations are simplified so that for layer j this yields

$$\int_{a_j}^{b_j} \left\{ \left(\lambda_j + 2\mu_j\right)\frac{\partial w_{r_j}}{\partial r}\frac{\partial u_{r_j}}{\partial r} + \lambda_j \frac{\partial w_{r_j}}{\partial r}\frac{u_{r_j}}{r} - 2\mu_j \frac{w_{r_j}}{r}\frac{\partial u_{r_j}}{\partial r} + \left[\mu_j k^2\gamma^2 + \mu_j \frac{2+n^2}{r^2} - \rho_j\omega^2\right] w_{r_j} u_{r_j} + in\left[\mu_j \frac{w_{r_j}}{r}\frac{\partial u_{\theta_j}}{\partial r} - \frac{\lambda_j}{r}\frac{\partial w_{r_j}}{\partial r} u_{\theta_j} - 3\mu_j w_{r_j}\frac{u_{\theta_j}}{r^2}\right] + ik\gamma\left[\mu_j w_{r_j}\frac{\partial u_{z_j}}{\partial r} - \lambda_j \frac{\partial w_{r_j}}{\partial r} u_{z_j}\right] \right\} dr = w_{r_j}\sigma_{rr_j}|_{b_j} - w_{r_j}\sigma_{rr_j}|_{a_j}, \tag{3a}$$

$$\int_{a_j}^{b_j} \left\{ \mu_j\left[\frac{\partial w_{\theta_j}}{\partial r}\frac{\partial u_{\theta_j}}{\partial r} - \frac{\partial w_{\theta_j}}{\partial r}\frac{u_{\theta_j}}{r}\right] - 2\mu_j\left[\frac{w_{\theta_j}}{r}\frac{\partial u_{\theta_j}}{\partial r} - w_{\theta_j}\frac{u_{\theta_j}}{r^2}\right] + \left[\left(\lambda_j + 2\mu_j\right)\frac{n^2}{r^2} + k^2\gamma^2\mu_j - \rho_j\omega^2\right] w_{\theta_j} u_{\theta_j} - in\left[\frac{\mu_j}{r}\frac{\partial w_{\theta_j}}{\partial r} u_{r_j} - \frac{\lambda_j w_{\theta_j}}{r}\frac{\partial u_{r_j}}{\partial r} - \left(\lambda_j + 4\mu_j\right) w_{\theta_j}\frac{u_{r_j}}{r^2}\right] + \frac{n}{r}\left(\lambda_j + \mu_j\right) k\gamma w_{\theta_j} u_{z_j} \right\} dr = w_{\theta_j}\sigma_{\theta r_j}|_{b_j} - w_{\theta_j}\sigma_{\theta r_j}|_{a_j}, \tag{3b}$$

$$\int_{a_j}^{b_j} \left\{ \mu_j \frac{\partial w_{z_j}}{\partial r}\frac{\partial u_{z_j}}{\partial r} - \frac{1}{r}\mu_j w_{z_j}\frac{\partial u_{z_j}}{\partial r} + \left[n^2\frac{\mu_j}{r^2} + k^2\gamma^2\left(\lambda_j + 2\mu_j\right) - \rho_j\omega^2\right] w_{z_j} u_{z_j} - ik\gamma\left[\mu_j \frac{\partial w_{z_j}}{\partial r} u_{r_j} - \lambda_j w_{z_j}\frac{\partial u_{r_j}}{\partial r} - \left(\lambda_j + \mu_j\right)\frac{w_{z_j} u_{r_j}}{r}\right] + nk\gamma\left(\lambda_j + \mu_j\right)\frac{w_{z_j} u_{\theta_j}}{r} \right\} dr = w_{z_j}\sigma_{z r_j}|_{b_j} - w_{z_j}\sigma_{z r_j}|_{a_j}. \tag{3c}$$

Here, λ and μ are the Lamé coefficients, and a_j and b_j are the inner and outer radius of layer j. Eq. (3) is valid for $j = 1$ to $m-1$, layer $j = m$ is covered in the next section. Note that a_1 is the inner radius of the pipe, which is set equal to zero for a rod in Section 3.

2.2. One dimensional equations for perfectly matched layer

Chew and Liu [30] demonstrated the existence of a PML for elastic waves and then introduced a complex coordinate stretching function to facilitate its introduction into the governing equations. This has become a popular method for applying a PML because it is relatively simple to integrate into standard finite element based formulations. Accordingly, coordinate stretching is applied here and, because the problem is axisymmetric, it is necessary to do this in only one [radial] dimension. Crucially, this means that the eigenexpansion in Eq. (2) remains valid for the PML region as well, and so the entire eigenproblem may be reduced from two dimensions to one. Accordingly, in the PML region ($j=m$) the radial coordinate r is replaced by a stretched coordinate $\tilde{r}$, defined as

$$\tilde{r} = \int_0^r \xi_r(s)\mathrm{d}s, \tag{4}$$

where ξ_r is a non-zero, continuous and complex-valued coordinate stretching function. This definition requires that

$$d\tilde{r} = \xi_r dr, \text{ and } \frac{\partial}{\partial \tilde{r}} = \frac{1}{\xi_r}\frac{\partial}{\partial r}. \tag{5}$$

The coordinate $\tilde{r}$ is then used to replace the coordinate r in Eq. (1) to form a revised set of governing equations and associated stress strain relations for the PML region. To derive the weak forms of the governing equations for the PML region, these equations are first multiplied by ξ_r, and then the inner products are weighted with an arbitrary function w_q in the same way as described in the previous section. Thus, for the PML region, where $j=m$, this yields

$$\int_{a_m}^{b_m} \left\{ (\lambda_m+2\mu_m)\frac{1}{\xi_r}\frac{\partial w_{r_m}}{\partial r}\frac{\partial u_{r_m}}{\partial r} + \lambda_m \frac{\partial w_{r_m}}{\partial r}\frac{u_{r_m}}{\tilde{r}} - 2\mu_m \frac{w_{r_m}}{\tilde{r}}\frac{\partial u_{r_m}}{\partial r} + \left[\mu_m k^2\gamma^2 + \mu_m\frac{2+n^2}{\tilde{r}^2} - \rho_m\omega^2\right]\xi_r w_{r_m} u_{r_m} \right.$$
$$\left. + \mathrm{i}n\left[\mu_m \frac{w_{r_m}}{\tilde{r}}\frac{\partial u_{\theta_m}}{\partial r} - \frac{\lambda_m}{\tilde{r}}\frac{\partial w_{r_m}}{\partial r}u_{\theta_m} - 3\xi_r\mu_m w_{r_m}\frac{u_{\theta_m}}{\tilde{r}^2}\right] + \mathrm{i}k\gamma\left[\mu_m w_{r_m}\frac{\partial u_{z_m}}{\partial r} - \lambda_m\frac{\partial w_{r_m}}{\partial r}u_{z_m}\right]\right\} dr = w_{r_m}\sigma_{rr_m}|_{b_m} - w_{r_m}\sigma_{rr_m}|_{a_m}, \tag{6a}$$

$$\int_{a_m}^{b_m} \left\{ \mu_m\left[\frac{1}{\xi_r}\frac{\partial w_{\theta_m}}{\partial r}\frac{\partial u_{\theta_m}}{\partial r} - \frac{\partial w_{\theta_m}}{\partial r}\frac{u_{\theta_m}}{\tilde{r}}\right] - 2\mu_m\left[\frac{w_{\theta_m}}{\tilde{r}}\frac{\partial u_{\theta_m}}{\partial r} - \xi_r w_{\theta_m}\frac{u_{\theta_m}}{\tilde{r}^2}\right] + \left[(\lambda_m+2\mu_m)\frac{n^2}{\tilde{r}^2} + k^2\gamma^2\mu_m - \rho_m\omega^2\right]\xi_r w_{\theta_m}u_{\theta_m} \right.$$
$$\left. - \mathrm{i}n\left[\frac{\mu_m}{\tilde{r}}\frac{\partial w_{\theta_m}}{\partial r}u_{r_m} - \frac{\lambda_m w_{\theta_m}}{\tilde{r}}\frac{\partial u_{r_m}}{\partial r} - (\lambda_m+4\mu_m)\xi_r w_{\theta_m}\frac{u_{r_m}}{\tilde{r}^2}\right] + \frac{n}{\tilde{r}}(\lambda_m+\mu_m)k\gamma\xi_r w_{\theta_m}u_{z_m}\right\} \mathrm{d}r = w_{\theta_m}\sigma_{\theta r_m}|_{b_m} - w_{\theta_m}\sigma_{\theta r_m}|_{a_m}, \tag{6b}$$

$$\int_{a_m}^{b_m} \left\{ \mu_m\frac{1}{\xi_r}\frac{\partial w_{z_m}}{\partial r}\frac{\partial u_{z_m}}{\partial r} - \frac{1}{\tilde{r}}\mu_m w_{z_m}\frac{\partial u_{z_m}}{\partial r} + \left[n^2\xi_r\frac{\mu_m}{\tilde{r}^2} + k^2\gamma^2\xi_r(\lambda_m+2\mu_m) - \rho_m\omega^2\xi_r\right]w_{z_m}u_{z_m} \right.$$
$$\left. - \mathrm{i}k\gamma\left[\mu_m\frac{\partial w_{z_m}}{\partial r}u_{r_m} - \lambda_m w_{z_m}\frac{\partial u_{r_m}}{\partial r} - (\lambda_m+\mu_m)\xi_r\frac{w_{z_m}u_{r_m}}{\tilde{r}}\right] + nk\gamma(\lambda_m+\mu_m)\frac{\xi_r}{\tilde{r}}w_{z_m}u_{\theta_m}\right\} \mathrm{d}r = w_{z_m}\sigma_{zr_m}|_{b_m} - w_{z_m}\sigma_{zr_m}|_{a_m}. \tag{6c}$$

Here, a_m and b_m are the inner and outer radius of the PML region.

2.3. The SAFE-PML eigenequation

Following the development of the weak forms of the governing equations for the layered elements of the pipe in Section 2.1, and the PML in 2.2, a finite element based eigensolution is obtained by discretising the displacement of an arbitrary mode in the radial direction, so that

$$u_q(r) = \sum_{i=1}^{p_q} \mathrm{N}_{qi}(r)u_{qi} = \mathbf{N}_\mathrm{q}\mathbf{u}_\mathrm{q} \tag{7}$$

where N_{qi} is a global trial (or shape) function, u_{qi} is the value of u_q at node i, and p_q is the number of nodes (or degrees of freedom) for the displacements in direction q. In addition, $\mathbf{N}_\mathrm{q}$ and $\mathbf{u}_\mathrm{q}$ are row and column vectors of length p_q, respectively, and it is also convenient to choose $\mathbf{N}_r = \mathbf{N}_\theta = \mathbf{N}_z = \mathbf{N}$. Isoparametric elements are used throughout this article, which requires that the weighting functions are equal to the shape functions so that $\mathbf{W}_r = \mathbf{W}_\theta = \mathbf{W}_z = \mathbf{N}$.

To generate a final governing eigenequation for the problem it is necessary to apply the boundary conditions of continuity of displacement and stress across the interface between each layer, as well as [for a pipe] a traction free condition at $r=a_1$ and $r=b_m$. Note that in the case of a solid rod (which is used as a benchmark in Section 3), the normal and shear stresses σ_{rr}, $\sigma_{\theta r}$ and σ_{zr} will vanish at the centre of the cylinder ($a_1=0$). The equations for these boundary conditions are not repeated here to save space, however an example of their application to related eigenproblems for both coated and uncoated pipes can be found in articles by Duan and Kirby [2], and Duan et al. [7]. Accordingly, following the introduction of these

boundary conditions, Eqs. (3) and (6) may be combined to yield the following eigenequation:

$$\begin{bmatrix} 0 & 0 & 0 & \mathbf{Z}_{1r}^{\mathrm{T}} & \mathbf{Z}_{2r}^{\mathrm{T}} & 0 \\ 0 & 0 & 0 & \mathbf{Z}_{1t}^{\mathrm{T}} & \mathbf{Z}_{2t}^{\mathrm{T}} & 0 \\ 0 & 0 & 0 & 0 & 0 & \mathbf{Z}_{3z}^{\mathrm{T}} \\ \mathbf{Z}_{1r} & \mathbf{Z}_{1t} & 0 & 0 & 0 & \mathbf{Z}_{1z} \\ \mathbf{Z}_{2r} & \mathbf{Z}_{2t} & 0 & 0 & 0 & \mathbf{Z}_{2z} \\ 0 & 0 & \mathbf{Z}_{3z} & \mathbf{Z}_{3r} & \mathbf{Z}_{3t} & 0 \end{bmatrix} \begin{Bmatrix} \boldsymbol{u}_r \\ \boldsymbol{u}_\theta \\ \boldsymbol{u}_z \\ \gamma \boldsymbol{u}_r \\ \gamma \boldsymbol{u}_\theta \\ \gamma \boldsymbol{u}_z \end{Bmatrix} = \gamma \begin{bmatrix} \mathbf{Z}_{1r}^{\mathrm{T}} & \mathbf{Z}_{2r}^{\mathrm{T}} & 0 & 0 & 0 & 0 \\ \mathbf{Z}_{1t}^{\mathrm{T}} & \mathbf{Z}_{2t}^{\mathrm{T}} & 0 & 0 & 0 & 0 \\ 0 & 0 & \mathbf{Z}_{3z}^{\mathrm{T}} & 0 & 0 & 0 \\ 0 & 0 & 0 & \mathbf{Z}_{1s} & 0 & 0 \\ 0 & 0 & 0 & 0 & \mathbf{Z}_{2s} & 0 \\ 0 & 0 & 0 & 0 & 0 & \mathbf{Z}_{3s} \end{bmatrix} \begin{Bmatrix} \boldsymbol{u}_r \\ \boldsymbol{u}_\theta \\ \boldsymbol{u}_z \\ \gamma \boldsymbol{u}_r \\ \gamma \boldsymbol{u}_\theta \\ \gamma \boldsymbol{u}_z \end{Bmatrix} \tag{8}$$

The matrices that make up this equation are listed in Appendix A. Eq. (8) is a sparse eigenequation and solution of this equation will deliver an unordered list of $n_T = 6p_q$ eigenmodes. This equation is solved here using the sparse eigensolver 'eigs' in MATLAB®, and the solution is executed on a laptop with a 2.4 GHz Intel Core™ CPU and 8 GB of RAM.

The solution of Eq. (8) delivers eigenmodes that belong to three different groups according to the way in which the energy in these modes propagates. These groups are summarised by Nguyen et al. [28] and their nomenclature is followed in this article. Thus, the first group contains the radiation modes and these are "standing waves in the transverse direction….that resonate mainly in the surrounding medium." The second group contains the trapped modes where the "energy is confined to the core of the waveguide without energy leakage into the surrounding medium." The third group contains the leaky modes and here "energy leaks into the surrounding medium" and the mode attenuates in the axial direction. Nguyen et al. note that one always obtains radiation and leaky modes after solution of the eigenproblem, whereas trapped modes are obtained "only if the bulk velocity in the guide is lower than the surrounding medium." Furthermore, it is the trapped and leaky modes that are of interest in non-destructive testing, as these modes propagate in the axial direction and so they play an important role in defect detection. Thus, the radiation modes are of little interest and so it is desirable to try and sort and remove these modes following the solution of Eq. (8). This may be achieved by following the method proposed by Nguyen et al. [28], who sort modes after first calculating the ratio of the energy propagating within the inner layers to that radiating into the PML. Accordingly, the energy ratio η is defined as

$$\eta = \frac{|\overline{E}_m|}{\sum_{j=1}^{m} |\overline{E}_j|} \tag{9}$$

where

$$\overline{E}_j = \frac{\omega^2}{2}\pi \int_{a_j}^{b_j} \rho_j \mathbf{u}_{\mathrm{q}}^* \bullet \mathbf{u}_{\mathrm{q}} r dr, \text{for } j = 1, m-1 \tag{10}$$

and

$$\overline{E}_m = \frac{\omega^2}{2}\pi \int_{a_m}^{b_m} \rho_m \mathbf{u}_q^* \bullet \mathbf{u}_q \, \tilde{r} \, \xi_r dr. \tag{11}$$

Through the careful choice of a value for η one may sort the eigenvalues to ensure that most or all of the radiation modes are removed. In this article labelling of the leaky and trapped modes will follow the convention established by Silk and Bainton [31], who defined torsional modes as $\mathrm{T}(0, n_c)$, longitudinal modes as $\mathrm{L}(0, n_c)$ and flexural modes as $\mathrm{F}(n, n_c)$, for $n > 0$ and $n_c > 0$; where n is the circumferential mode order defined in Eq. (2). Note that for buried waveguides an additional family of longitudinal and flexural modes appear and these are labelled $\mathrm{L}(0, n_c)'$and $\mathrm{F}(n, n_c)'$[19]. The $\mathrm{L}(0, n_c)'$modal family has a similar mode shape to the $\mathrm{L}(0, n_c)$ family, however they appear because of the coupling between the waveguide and the surrounding medium. At low frequencies the $\mathrm{L}(0, n_c)$ and $\mathrm{F}(n, n_c)$ modes are generally leaky type modes, whereas the $\mathrm{L}(0, n_c)'$and $\mathrm{F}(n, n_c)'$modes are radiation type modes. As the frequency increases their behaviour tends to reverse, so that at high frequencies $\mathrm{L}(0, n_c)'$and $\mathrm{F}(n, n_c)'$are generally found to be leaky modes.

3. Application to buried rods

The PML plays a very important role in determining the speed and accuracy of the solution to the eigenproblem derived in the previous section. This in turn depends on the thickness of the PML layer, as well as the choice of coordinate stretching function. Clearly, the identification of an optimal coordinate stretching function is crucial in reducing the thickness of the PML, and many different coordinate stretching functions are discussed in the literature. A useful review of coordinate stretching functions for the Helmholtz equation is provided by Cimpeanu et al. [32]. Michler et al. [33] also provide a comprehensive review for a number of wave propagation problems. Numerous other articles on coordinate stretching functions are available in the literature and this reflects the fact that the choice of an appropriate stretching function is often highly problem dependent and this is not always straightforward [32,34]. However, it is interesting to note that most of

these articles choose to use a similar type of stretching function, which normally takes the form of a polynomial [32–35], where

$$\xi(x)=\begin{cases}1 & \text{if } x\le L_1\\ 1+\frac{s_1}{ik}\left(\frac{x-L_1}{h}\right)^{s_2} & \text{if } x\ge L_1\end{cases}. \tag{12}$$

Here, x represents an arbitrary coordinate system, so that $x=L_1$ is the location of the entrance into the PML, h is the width of the PML, and s_1 and s_2 are real valued constants that are chosen by the user and tuned for a particular problem. The challenge lies in choosing the best values for s_1 and s_2 for a particular problem and this can require repetitive calculations before identifying suitable values.

The coordinate stretching function in Eq. (12) is normally used to terminate problems involving wave propagation. This explains the presence of the wavenumber k, because the performance of the PML will be strongly correlated to excitation frequency in wave propagation problems. However, in eigenproblems the excitation frequency is not necessarily so important because one is more concerned with accurately capturing mode shapes and these are not so strongly correlated with frequency. Accordingly, in their study on open elastic waveguides, Nguyen et al. [28] modified this stretching function and used

$$\xi(x)=1+\alpha_p\left(1-i\beta_p\right)\left(\frac{x-L_1}{h}\right)^2, \tag{13}$$

where, α_p and β_p are additional real valued constants. It is interesting to note that Nguyen et al. retain a polynomial structure and they demonstrate that this coordinate stretching function works well for their particular problem. However, there is no reason why a polynomial stretching function should be optimal for the type of problem studied here, and it is interesting to note that Singer and Turkel [36] speculate that "when evanescent waves are present [in a wave propagation problem] it may be more advantageous to use an exponential fit." This appears to be relevant to eigenproblems and so an alternative exponential coordinate stretching function is investigated here to see if this is better suited to the analysis of buried pipes. Accordingly, the following alternative coordinate stretching function is proposed:

$$\xi_r(r)=e^{\alpha\tilde{r}}-i\left[e^{\beta\tilde{r}}-1\right] \tag{14}$$

where $\tilde{r}=(r-a_m)/h$, so that the thickness of the PML layer is $h=b_m-a_m$, and α and β are real valued constants. This stretching function is designed to deliver a smooth valued function that decays exponentially with distance from the entrance to the PML.

To investigate the choice of stretching function a steel rod embedded in concrete is examined first, as this is a demanding problem studied by Castaings and Lowe [19], and later by Nguyen et al. [28]. For this example, the steel rod forms the inner layer and the outer PML layer abuts directly onto the rod so that the PML takes on the properties of concrete. Solutions to Eq. (8) are then obtained using three noded line elements with a constant width of 1 mm, so that the number of elements increases as the thickness of the PML is increased. This delivers a high mesh density so that one may focus on the effect of the length of the PML. The diameter of the steel rod is 10 mm, and for steel $c_{T_1}=3260$ m/s, $c_{L_1}=5960$ m/s, and $\rho_1=7932$ kg/m^3; for concrete, $c_{T_m}=2637.5$ m/s, $c_{L_m}=4222.1$ m/s, and $\rho_m=2300$ kg/m^3 [19,28]. To investigate convergence a very low excitation frequency is chosen because longer wavelengths cause significant problems for PMLs. Accordingly, the first parameter to be investigated is the thickness of the PML layer, and in Table 1 the convergence of the polynomial stretching function proposed by Nguyen et al. [28] is investigated, so that values of $\alpha_p=3$ and $\beta_p=4$ are used in Eq. (13). In Table 1, the wavenumbers for the first two axisymmetric modes are presented and it is clear that the rate of convergence depends on the mode being analysed. For example, the first longitudinal mode L(0,1) converges when h/b_1 is equal to or greater than eight; whereas good convergence for the first torsional mode T(0,1) is obtained for $h/b_1=2$. This is because the radial wavelength of L(0,1) is 251 mm at 10 kHz, whereas the equivalent wavelength for T(0,1) is 60 mm. It is interesting to note, however, that even for a polynomial stretching function the one dimensional approach means that it is

Table 1
Eigenvalues for steel rod using polynomial stretching function [22] at 10 kHz.

h/r_b	Wavenumber γ		n_T	CPU time (s)
	L(0,1)	T(0,1)		
1	0.93000–1.38074i	1.40449–5.30741i	246	0.15
2	0.76987–1.08198i	1.40752–5.30617i	366	0.24
3	0.92212–1.19420i	1.40752–5.30617i	486	0.27
4	0.86554–1.13582i	1.40752–5.30617i	606	0.29
6	0.88605–1.13233i	1.40752–5.30617i	846	0.36
8	0.88535–1.13025i	1.40752–5.30617i	1086	0.62
10	0.88521–1.13034i	1.40752–5.30617i	1326	0.76
12	0.88522–1.13035i	1.40752–5.30617i	1566	1.23
15	0.88522–1.13035i	1.40752–5.30617i	1926	1.72

possible to obtain a fully converged solution at low frequencies. Moreover, this is achieved with a solution time that is less than 1 s, even for a relatively large PML. Note that the solution time recorded in Table 1 also includes the sorting and discarding of radiation modes, as well as the calculation of energy velocity for each mode.

The solutions presented in Table 1 show that even for a relatively small waveguide it is necessary to use values of $h/b_1 = 8$ and above to obtain satisfactory convergence for L(0,1). This is likely to present problems when moving to larger geometries such as those encountered with pipelines. Therefore, it is desirable to obtain faster convergence and the only way to do this is to improve the efficiency of the coordinate stretching function. Accordingly, in Table 2 the exponential coordinate stretching function proposed in Eq. (14) is compared against the polynomial stretching function of Nguyen et al. [28] for different values of α_p , β_p, α and β. For purposes of comparison, the width of the PML is chosen to be $h = b_1$. In Table 2 it is evident that the polynomial stretching function has not converged for a PML of thickness $h = b_1$, even after attempting to optimise values for α_p and β_p. However, the exponential stretching function is seen to deliver much better performance and appears to offer the potential to improve the PML, at least for this particular problem.

To further investigate the performance of an exponential stretching function, the frequency of the problem is increased to 160 kHz, whilst maintaining $h = b_1$. This problem is chosen because L(0,1) and L(0,1)′ both have a phase velocity that is very close to the longitudinal phase velocity of the surrounding medium at 160 kHz. This means that the radial wavelength will be long and so a frequency close to 160 kHz represents a worst case scenario at higher frequencies. The accuracy of the exponential stretching function is investigated in Tables 3a and 3b, in which the relative error is calculated by dividing the wavenumber computed when $h = b_1$ with the equivalent value obtained using a polynomial stretching function with $h = 10b_1$. In Table 3a it is seen that at higher frequencies, high levels of accuracy are achieved for T(0,1) and L(0,1), even when $h = b_1$. This is because these modes have a smaller radial wavelength at higher frequencies, which for this problem is 25 mm for T(0,1) and 65 mm for L(0,1). In contrast the radial wavelength is 139 mm for L(0,1)' and 28 mm for L(0,2), and it is important also to note that the radiation angle for L(0,1)′ is 80° at this frequency. This means that accurately predicting the wavenumber for L(0,1)' is far more challenging and one can see that solution accuracy starts to drop in Table 3b. This drop in accuracy can, of course, be addressed by increasing the thickness of the PML, although it is seen that it is still possible to get some good results with $h = b_1$ when using an exponential stretching function. The results reported in Tables 3a and 3b do,

Table 2
Influence of stretching function on eigenvalues for steel rod with $h/r_b = 1$ at 10 kHz.

Stretching function	α	β	Wavenumber γ		Relative error (%)	
			L(0,1)	T(0,1)	L(0,1)	T(0,1)
Polynomial	3	4	0.93000–1.38074i	1.40449–5.30741i	17.72	0.06
Polynomial	6	6	0.90385–1.11178i	1.40781–5.30633i	1.83	0.006
Exponential	3	4	0.90090–1.19314i	1.40758–5.30616i	4.51	0.001
Exponential	3	5	0.88525–1.13032i	1.40766–5.30619i	0.003	0.003
Exponential	4	5	0.88418–1.12890i	1.40766–5.30600i	0.12	0.004

Table 3a
Eigenvalues for steel rod with $h/r_b = 1$ at 160 kHz.

Stretching function	α	β	Wavenumber γ		Relative error (%)	
			L(0,1)	T(0,1)	L(0,1)	T(0,1)
Polynomial	3	4	0.95015–0.09069i	0.76487–0.10978i	<0.001	0.52
Polynomial	6	6	0.95012–0.09069i	0.76349–0.11034i	<0.001	0.01
Exponential	3	4	0.95016–0.09069i	0.76344–0.11005i	<0.001	0.27
Exponential	3	5	0.95015–0.09069i	0.76348–0.11024i	<0.001	0.10
Exponential	4	5	0.95015–0.09067i	0.76416–0.10950i	0.02	0.77

Table 3b
Eigenvalues for steel rod with $h/r_b = 1$ at 160 kHz.

Stretching function	α	β	Wavenumber γ		Relative error (%)	
			L(0,1)′	L(0,2)	L(0,1)′	L(0,2)
Polynomial	3	4	0.83091–0.04478i	0.54802–0.36943i	29.6	0.003
Polynomial	6	6	0.85053–0.03388i	0.54804–0.36943i	46.7	0.003
Exponential	3	4	0.84532–0.06237i	0.54812–0.36964i	1.9	0.06
Exponential	3	5	0.85539–0.04796i	0.54814–0.36916i	24.6	0.07
Exponential	4	5	0.84368–0.06348i	0.54935–0.36835i	0.19	0.29

however, demonstrate that the optimum choice for a PML is problem dependent and so one must reach a compromise that works well over a wide range of parameters. In this respect, the exponential solution with $\alpha=4$ and $\beta=5$ performs best over the two sets of tests carried out here; however, it must also be remembered that these tests are designed to cover two extremes of the frequency spectra and they deliberately pick areas where the choice of PML is difficult. Outside of the frequency range chosen here all of these coordinate stretching functions generally perform well. This can be seen in Fig. 2, where the relative error in the prediction of the wavenumber for a steel rod surrounded by concrete is presented over a wide frequency range using the exponential solution with $\alpha=4$ and $\beta=5$. The relative error in Fig. 2 is presented for a PML of thickness $h=b_1$, as well as $h=4b_1$, with the error calculated relative to a solution obtained using a polynomial stretching function with $h=10b_1$. It is clear from Fig. 2 that for this problem the exponential stretching function works well over a wide frequency range, even for $h=b_1$, and this includes those frequency extremes examined previously. Furthermore, it is evident that increasing the width of the PML significantly improves the accuracy for each mode, so that for $h=4b_1$ it is possible to obtain high levels of accuracy across the frequency domain.

The numerical experiments carried out previously demonstrate that high levels of accuracy may be achieved using a one dimensional mesh coupled with an exponential stretching function. This method is now further validated through the calculation of dispersion curves for the embedded rod studied above, and in order to provide confidence in the accuracy of these predictions a PML of width $h=4b_1$ is used. Accordingly, Fig. 3a and b present the dispersion curves for a 10 mm rod buried in concrete, where the phase velocity is defined as $c_p=\mathrm{Re}(c_T/\gamma)$ and the attenuation as $\Delta=-8.686\mathrm{Im}(k\gamma)$. An exponential coordinate stretching function is used, with $\alpha=4$ and $\beta=5$; for the finite element mesh, 10 elements are used in the rod and 40 elements in the PML region. This delivers a final eigenequation with $n_T=606$ degrees of freedom, which takes 1.31 s to compute for a single frequency, including the time spend sorting the computed eigenmodes. The dispersion curves in Fig. 3a and b present only those modes of interest in non-destructive testing and so radiation modes are omitted. This is achieved by discarding all modes with an energy ratio above 0.9 [see Eq. (9)], and this is why some modes are discontinuous in these plots, as they move from being a predominantly leaky mode to a predominantly radiation mode, or vice versa. Following this, the dispersion curves in Fig. 3a and b are seen to match the analytic solutions generated by Castaings and Lowe [19], and they also compare very well with the solutions obtained by Nguyen et al. [28].

It is interesting to note that both Castaings and Lowe [19], and Nguyen et al. [28] suggest that the phase velocity of a leaky mode cannot cross the bulk velocity of the surrounding medium. In view of this Nguyen et al. [28] queried the accuracy of their results at low frequencies, where their predictions for L(0,1) were seen to cross the bulk velocity of the surrounding medium. However, behaviour identical to that observed by Nguyen et al. [28] is also seen in Fig. 3a, where the phase velocity for L(0,1) is seen to drop below the bulk velocity (equal to 4222.1 m/s) at about 12 kHz. If one examines Table 1 then it is evident that good convergence is achieved for L(0,1) at 10 kHz, and there is no evidence here to suggest that computational error is the reason for this behaviour. It is also noted that at 10 kHz the real part of $k\gamma$ is 17.06 m^{-1} for L(0,1), which is larger than $\omega/c_{L_m}(=14.88\ \mathrm{m}^{-1})$, and so in this example the phase velocity is significantly lower than the bulk velocity of the surrounding medium. Crucially, however, for this mode $k\gamma$ has an imaginary part that is larger than its real part and so the radial wavenumber may take on a positive real part and a positive imaginary part. Accordingly, this mode conforms to the normal definition of a leaky mode and so it is concluded here that this mode is indeed physically correct.

4. Application to buried pipes

The main focus of this article is the non-destructive testing of buried pipelines and so in this section wave propagation in buried pipes that are either coated or uncoated is investigated. To do this, an 8 in. schedule 40 pipe is chosen, as this is a relatively large pipe and this geometry has also recently been studied by Leinov et al. [11,12]. An 8 in. schedule 40 pipe has

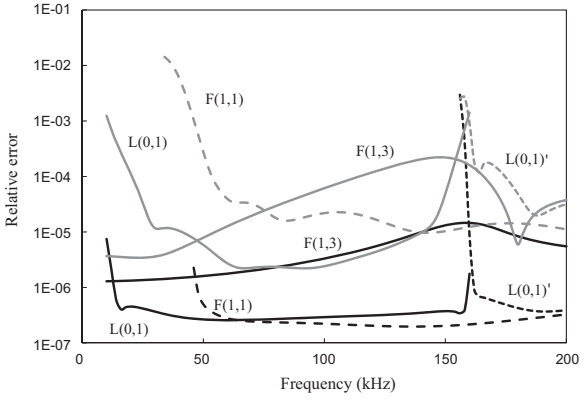

Fig. 2. Relative error of the model using an exponential stretching function with $\alpha=4$ and $\beta=5$. ——, $h/r_b=1$; ——, $h/r_b=4$.

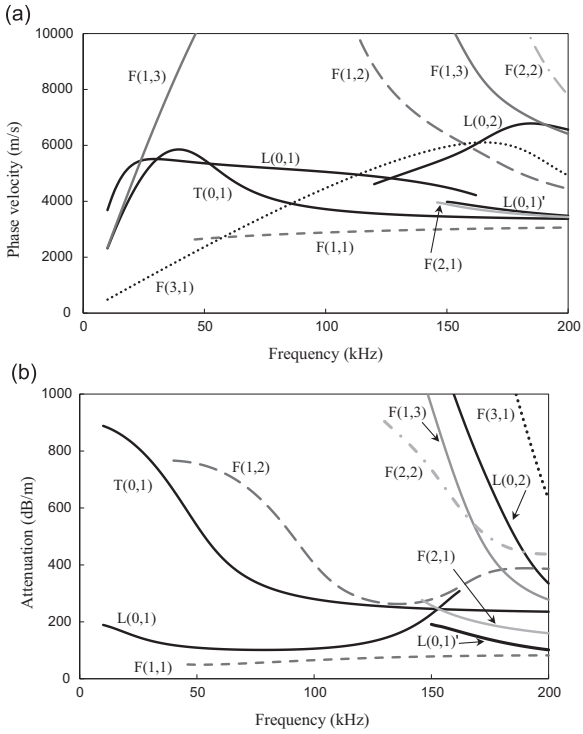

Fig. 3. Dispersion curves for steel rod embedded in concrete, with $\alpha = 4$ and $\beta = 5$ and $h/r_b = 4$. (a) phase velocity; (b) attenuation.

an outer radius $b_1 = 109.54$ mm, and an inner radius $a_1 = 101.36$ mm, with $c_{T_1} = 3260$ m/s, $c_{L_1} = 5960$ m/s, and $\rho_1 = 7932$ kg/m^3. To investigate the suitability of an exponential stretching function for this type of problem, the pipe is buried in two different media: dry sand and soil. The properties for dry sand are $c_{T_m} = 105$ m/s, $c_{L_m} = 800$ m/s, and $\rho_m = 1620$ kg/m^3 [11], and for soil $c_{T_m} = 300$ m/s, $c_{L_m} = 1540$ m/s, and $\rho_m = 2000$ kg/m^3 [4]. The properties of a viscoelastic coating are defined here as $c_{T_2} = 1/\left[\frac{1}{\tilde{c}_T - i\tilde{\alpha}_T}\right]$ and $c_{L_2} = 1/\left[\frac{1}{\tilde{c}_L - i\tilde{\alpha}_L}\right]$, where $\tilde{c}_T$ and $\tilde{c}_L$ denote shear and longitudinal phase velocities, respectively, and $\tilde{\alpha}_T$ and $\tilde{\alpha}_L$ represent the shear and longitudinal attenuation in the coating [37]. Following Duan et al. [7], a bitumen coating with a thickness of 1.5 mm is analysed, so that $\tilde{c}_T = 750$ m/s, $\tilde{c}_L = 1860$ m/s, $\tilde{\alpha}_T = 3.9 \times 10^{-3}$ s/m, $\tilde{\alpha}_L = 0.023 \times 10^{-3}$ s/m, and $\rho_2 = 1200$ kg/m^3. Further, a minimum of 21 nodes per wavelength is maintained up to a frequency of 120 kHz, and an exponential coordinate stretching function with $\alpha = 4$ and $\beta = 5$ is adopted and the PML width is $h = b_1 - a_1$. This generates $n_T = 2406$ degrees of freedom and it takes 0.9 s to solve for and sort the eigenmodes at each frequency.

4.1. Uncoated and coated pipe buried in sand

In the previous section, the PML model was validated for a buried rod. Therefore, in this section it is necessary to start by validating the model for a buried pipe and so in Fig. 4 the convergence of the PML model is investigated for an uncoated 8 in. schedule 40 pipe buried in sand. In Fig. 4a PML of width $h = b_1 - a_1$ is used and the relative error is found by dividing these predictions by those predictions obtained using a polynomial stretching function with $h = 10(b_1 - a_1)$. It is seen in Fig. 4 that the convergence obtained for the exponential stretching function is very good across the entire frequency range, and this significantly outperforms the polynomial stretching function at lower frequencies. Accordingly, this exponential stretching function is now used to generate dispersion curves for an uncoated 8 in. schedule 40 pipe, and these predictions are compared against analytic predictions obtained using the commercial software DISPERSE [9,11]. Fig. 5 is also designed to replicate those predictions reported by Leinov et al. [11], and so "group" velocity and attenuation are presented for T(0,1) and L(0,2). It is evident in Fig. 5 that the SAFE-PML predictions deliver excellent agreement with DISPERSE across the entire frequency range, even for a PML that has a width equal to the thickness of the pipe wall. This provides further validation of the SAFE-PML approach introduced here, and demonstrates that predictions may be obtained for buried pipes using a relatively thin PML.

The SAFE-PML model is now used to investigate the effects of a coating on the propagation of elastic waves in buried pipes. A recent article by Leinov et al. [12] reported that "isolation" effects may appear whereby particular modes in coated pipes leak less energy into the surrounding medium when compared to uncoated pipes. This is an interesting finding that has ramifications for LRUT and so this effect is explored in more detail in this section. Accordingly, an 8 in. schedule 40 pipe

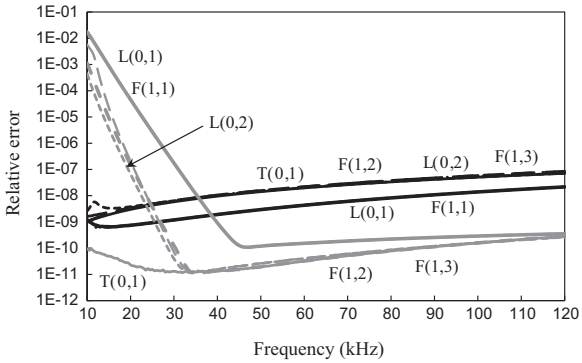

Fig. 4. Relative error for an 8 in. shedule40 pipe buried in sand. ——, exponential stretching function ($\alpha=4, \beta=5$); ——, polynomial stretching function ($\alpha_p=3, \beta_p=4$).

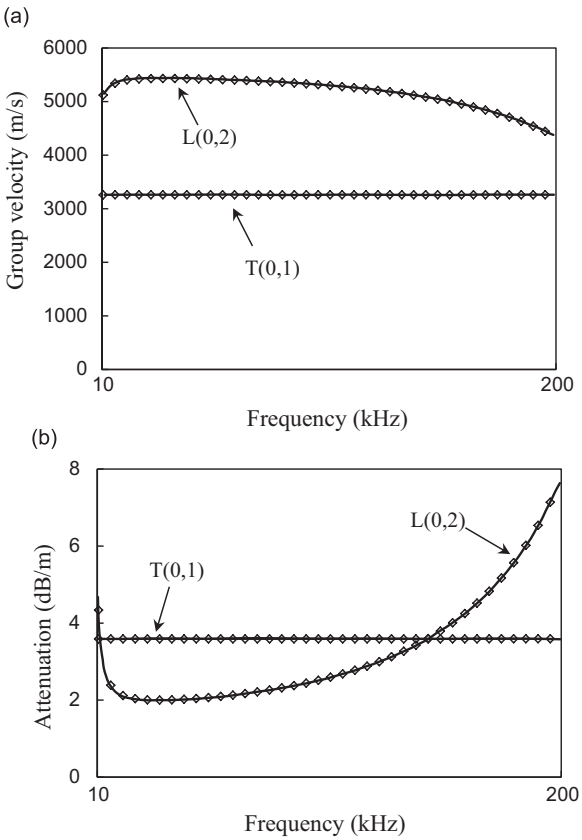

Fig. 5. Dispersion curves of zeroth order modes for steel pipe embedded in dry sand; (a) group velocity; (b) attenuation. ◊ , current numerical solution; ——, Global Matrix (DISPERSE) solution [11].

coated with bitumen and buried in sand is studied here (see the start of this section for geometry and material properties). The attenuation of different eigenmodes is presented in Fig. 6(a) to (c), and in order to view the effects of the coating predictions are also presented for the equivalent uncoated pipe. Note that for large pipes the number of leaky modes present at normal LRUT frequencies is substantial and if one plotted all of these modes over a wide frequency range then the attenuation plots would be unintelligible. Thus, in Fig. 6 only those modes that have low levels of attenuation are included, as these are most relevant in non-destructive testing. Furthermore, predictions are grouped into "families" of modes, so that the T(0,1) family contains T(0,1), F(1,2) and F(2,2); the L(0,1) family contains L(0,1), F(1,1,) and F(2,1); and the L(0,2) family contains L(0,2), F(1,3) and F(2,3) [7].

If one first examines the attenuation in a buried pipe without a coating in Fig. 6, then it is evident that relatively large levels of attenuation are present as energy radiates from these modes into the surrounding medium. It is interesting to note

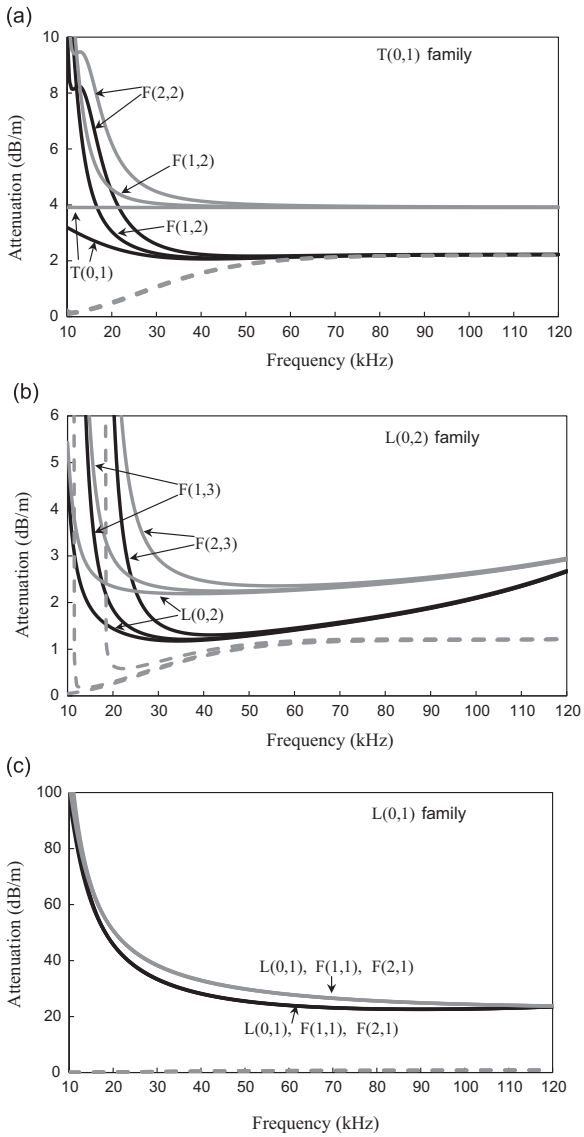

Fig. 6. Attenuation in an 8 in. pipe embedded in sand, with $\alpha = 4$ and $\beta = 5$ and $h = b_1 - a_1$: (a) T(0,1) family (b), L(0,2) family, (c) L(0,1) family. ——, pipe coated and buried; ——, pipe buried only; - - -, pipe coated only.

that very high levels of attenuation are seen for the L(0,1) family, and the large difference between this and the T(0,1) and L(0,2) families is believed to be because of the different mode shapes belonging to each family. For example, the L(0,1) family typically has a strong displacement in the radial direction for the parameters shown in Fig. 6, see also the mode shapes presented by Duan and Kirby [7] for the same [unburied] pipe at 70 kHz. A strong radial displacement means that the L(0,1) family couples efficiently to the surrounding medium and so high levels of energy radiates from the pipe and these modes are strongly attenuated. In contrast, the radial displacement patterns for the T(0,1) and L(0,2) families are relatively weak, which means that the coupling between the coated pipe and sand is reduced and so less energy from the T(0,1) and L(0,2) families radiates into the sand. This is believed to be the reason why the different modal families exhibit such different levels of attenuation, and serves to illustrate the importance of mode shape in explaining modal behaviour in buried pipes.

The addition of a coating is seen to reduce the attenuation of each mode in Fig. 6(a)–(c). This effect has recently been observed by Leinov et al. [12] following the addition of a Polyethylene (PE) viscoelastic coating with a thickness of 19 mm. Accordingly, the predictions obtained here support the findings of Leinov et al., and it is interesting also to compare the relative levels of "isolation" achieved in each study. To enable this, the attenuation of an unburied coated pipe is also shown in Fig. 6(a–(c). This shows that for the T(0,1) family good isolation is achieved in the medium to high frequency range, whereas for the L(0,2) family the isolation remains limited to the mid frequency range. In contrast, for the L(0,1) family the difference in the level of attenuation between a buried and unburied coated pipe is very large across the entire frequency range. That is, the L(0,1) family does not exhibit the same behaviour as that seen for T(0,1) and L(0,2), and so one cannot

conclude that isolation is a general effect that applies to all modes. It is proposed that the difference in behaviour seen for different families of modes can again be explained by the mode shapes that are common to, and indeed define, each modal family. For instance, in the medium to high frequency range the presence of the coating means that the displacement for the T(0,1) and L(0,2) is relatively low at the edge of the coating [7] and this means that little energy radiates from the coating. However, at lower frequencies the coating is less effective (seen in a reduction in attenuation for the unburied coated pipe) and so the amplitude of displacement is proportionally higher within the coating and more energy leaks out. In contrast, the displacement pattern of the L(0,1) family remains relatively high at the edge of the coating over the entire frequency range, especially in the radial direction [7], so that high levels of energy radiate out of the pipe for all of these modes. That is, if the effect of a coating is to lower significantly the modal displacement pattern within the coating region, then the energy radiated into a surrounding medium will be small and the attenuation of a buried coated pipe will tend towards that of an unburied coated pipe and this will "isolate" the pipe. Conversely, if the effect of the coating is reduced, for example when the frequency is lowered for bitumen, then the attenuation in a coated buried pipe will tend towards the behaviour seen for an uncoated buried pipe and the pipe is no longer isolated.

The "isolation" imparted by the coating described above was also observed experimentally by Leinov et al. [12] for T(0,1) and L(0,2) at frequencies between about 10 kHz and 40 kHz. Leinov et al. measured levels of attenuation that are lower than those observed here and this is seen to extend to frequencies below those observed in Fig. 6(a) to (c). Leinov et al. propose that the isolation effect observed in their measurements is determined by the "impedance" of their viscoelastic material relative to that of sand, such that low relative values of impedance for the viscoelastic coating delivers effective isolation. For a viscoelastic material there are two [complex] values for impedance, although Leinov et al. choose to define their impedance using only the real part of the shear properties. If one adopts their definition for impedance it is observed that the impedance of the bitumen studied here is 34 times that of the PE used by Leinov et al., and it is 5.3 times that of sand. However, isolation effects are still observed for bitumen, albeit over a higher frequency range when compared to that seen by Leinov et al. Accordingly, it appears likely that these isolation effects are related to a range of parameters and that they are not limited solely to the relative impedance of the coating and the surrounding material (where the impedance is defined as the real part of the shear properties). These parameters are likely to include the acoustic properties of each material (both shear and longitudinal), the density of each material, the thickness of the coating, the frequency of excitation, and the mode of interest. For example, Leinov et al. [12] demonstrate that by choosing a material that is much less attenuative than bitumen, and also increasing the width of this material to 19mm, then it is possible to achieve good isolation for T(0,1) and L(0,2) at relatively low frequencies. This choice of parameters also enables Leinov et al. to provide lower levels of attenuation than that seen for bitumen in this current study. Accordingly, it appears to be possible, through careful choice of a coating material for a given application, to optimise levels of attenuation for a particular mode over a chosen frequency range. However, this isolation effect is not limited to low impedance materials, and may also be observed in other viscoelastic materials that are common in pipeline applications, such as bitumen. Therefore, in order to optimise the levels of isolation provided by a coating for a given application, the evidence presented here suggests that one needs first to start by analysing the modal displacement patterns for the coupled system, and to do this for the individual mode and frequency range of interest.

4.2. Uncoated and coated pipe buried in soil

The purpose of this article is to illustrate an efficient method for finding the eigenmodes for a buried pipe. Therefore, it is necessary to show that the method works for a number of common scenarios. Accordingly, the method is also validated here for a large pipe buried in soil, which is another common surrounding for pipelines. The properties of soil were given in the introduction to this section, and the exponential stretching function and finite element mesh specified in the previous section are also applied here. The accuracy of the exponential stretching function is compared against a polynomial stretching function for soil in Fig. 7, and it is seen that similar levels of accuracy are also obtained

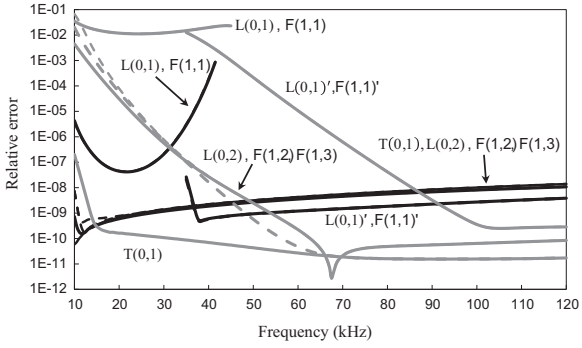

Fig. 7. Relative error of the model for an 8 in. shedule40 pipe buried in soil. ——, exponential stretching function; ——, polynomial stretching function.

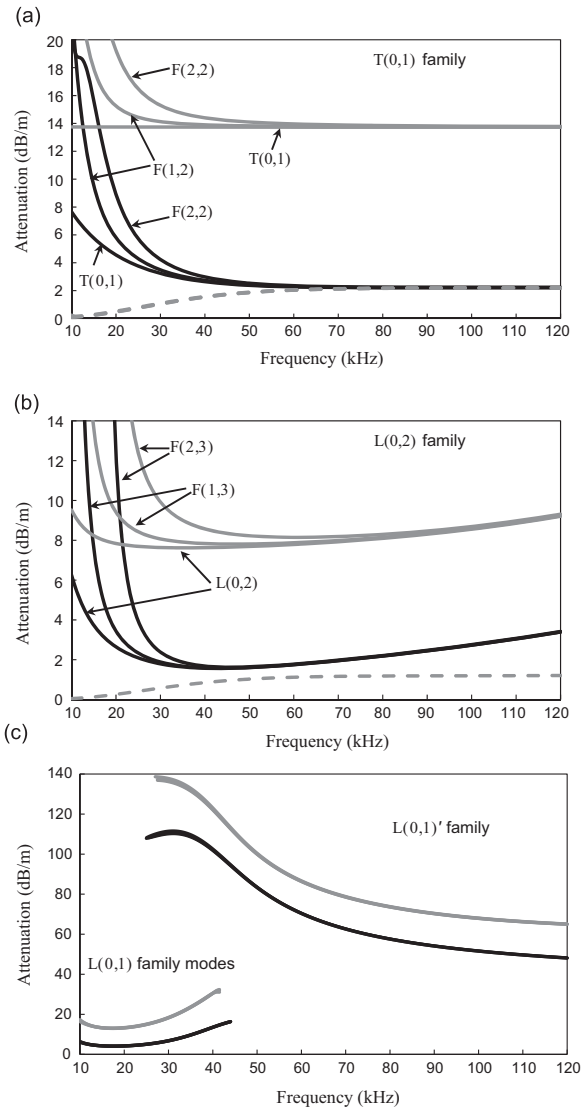

Fig. 8. Attenuation curves for 8inch pipe embedded in soil, with $\alpha = 4$ and $\beta = 5$ and $h = b_1 - a_1$. ——, pipe coated and buried; ——, pipe buried only; - - -, pipe coated only.

here for soil, although the accuracy is reduced for the L(0,1) family of modes. This is because the radial wavelength in soil is longer than for sand and this makes it more difficult for the PML to absorb energy at lower frequencies. One can clearly see that this causes additional problems for the polynomial stretching function and that some advantages are obtained by using the exponential function for soil. In Fig. 8(a)–(c) it is evident that a pipe buried in soil behaves in a similar way to one buried in sand, although for an uncoated pipe more energy leaks into the soil. This means that when a coating is added, the "isolation" effect induced by this coating is far more significant than that seen for sand. It is interesting also to note that the levels of attenuation for a coated pipe buried in soil or sand are similar to one another, at least for the T(0,1) and L(0,2) family of modes. This further illustrates that the drop in attenuation is caused by the coating itself. Moreover, the only significant difference seen between the behaviour for soil and sand is the attenuation of the L(0,1) family, where a discontinuity is apparent as the modes change from leaky to radiation, or vice versa for the $L(0,1)'$ family. However, for applications in long range ultrasonic testing it is the T(0,1) and L(0,2) modes that are widely used, and the isolation behaviour imparted by the coating on these two modes is seen to provide a consistent effect for both sand and soil. Thus, it is seen that the observations of Leinov et al. [12] are applicable over a wide range of parameters and for different surrounding materials, and so it appears possible to plan to take advantage of this effect when undertaking long range ultrasonic testing on buried coated pipes.

5. Conclusions

This article presents a numerical method for computing the eigenmodes for a multi-layer embedded axisymmetric waveguide. The article uses a Galerkin based approach to derive a one dimensional version of the SAFE formulation, which is then closed using a one dimensional PML. This approach is designed to offer a PML based alternative to the one dimensional SAFE formulations that use infinite elements [20], or numerical dashpots [22]. The use of a PML means that the problem can readily be tackled using a standard FE based approach, and this facilitates an investigation into different coordinate stretching functions. It is shown that an exponential stretching function is more computationally efficient when compared to the more traditional polynomial coordinate stretching function, at least for the problems examined in this article. Furthermore, this permits the use of a relatively thin PML and it is shown that accurate results may be obtained over a wide frequency range using a PML of thickness equal to the thickness of the pipe wall, or the radius of a rod. This enables eigenmodes to be obtained and sorted at frequencies up to 120 kHz in under about 1 second for each frequency. Accordingly, the technique presented here is sufficiently fast and accurate to be suitable for use in the development of "hybrid" models that have been applied previously to the analysis of scattering from defects [2,7,16].

The one-dimensional SAFE-PML model is applied here to coated and uncoated pipes. For uncoated pipes buried in sand or soil, it is seen that the attenuation of each mode is high, as energy radiates out of the pipe into the surrounding medium. This is likely to have a significant and detrimental impact on non-destructive testing methodologies. However, when a coating is applied the coating will, under particular conditions, isolate the pipe by concentrating the energy propagation within the walls of the pipe and the coating. This is observed here for bitumen with a thickness of 1.5 mm, and this effect is the same as the isolation imparted by a thick layer of PE recently observed by Leinov et al. [12]. However, it is noted that this isolation effect depends on the mode, or modes, that are being analysed, the properties and geometry of the viscoelastic coating and surrounding medium, as well as the frequency range being studied. This is because the ability of a mode to radiate energy into the surrounding medium [and hence to undergo high levels of attenuation] is linked to the shape of a given eigenmode. Those modes with a relatively high displacement within the coating region, especially in the radial direction, will radiate energy more effectively than those in which the displacement drops within the coating. For bitumen, the effect of the coating on each eigenmode is seen to limit isolation to the medium and high frequency range for T(0,1), and the medium frequency range for L(0,2). However, Leniov et al. [12] show that by choosing a different viscoelastic material one may achieve good levels of isolation in the lower frequency range. Therefore, the results presented here demonstrate that most viscoelastic coatings are likely to provide some degree of isolation from their surrounding medium, and this includes those materials typically found in pipeline applications. This will help in the application of non-destructive testing in buried pipelines, as under certain conditions one is limited only by the attenuation properties of the coating and not the surrounding medium; however, the degree of isolation provided by a coating will depend on many parameters relating to material properties and excitation frequency, and one cannot always be sure that levels of isolation will be maintained if one or more of these parameters is changed.

Appendix A

For a buried pipe with an arbitrary number of $m-1$ layers, then

$$\mathbf{Z}_{1r} = \sum_{j=1}^{m} \left[\left(\lambda_j + 2\mu_j\right)\mathbf{K}_{1j} + \lambda_j \mathbf{K}_{2j} + \mu_j (n^2+2)\mathbf{K}_{6j} - 2\mu_j \mathbf{K}_{2j}^{\mathrm{T}} - \rho_j \omega^2 \mathbf{K}_{4j} \right] \tag{A1}$$

$$\mathbf{Z}_{1t} = \mathrm{i}n \sum_{j=1}^{m} \left[\mu_j \mathbf{K}_{2j}^{\mathrm{T}} - 3\mu_j \mathbf{K}_{6j} - \lambda_i \mathbf{K}_{2j} \right] \tag{A2}$$

$$\mathbf{Z}_{1z} = \mathrm{i}k \sum_{j=1}^{m} \left[\mu_j \mathbf{K}_{3j} - \lambda_j \mathbf{K}_{3j}^{\mathrm{T}} \right] \tag{A3}$$

$$\mathbf{Z}_{1s} = -k^2 \sum_{j=1}^{m} \mu_j \mathbf{K}_{4j} \tag{A4}$$

$$\mathbf{Z}_{2r} = -\mathrm{i}n \sum_{j=1}^{m} \left[\mu_j \mathbf{K}_{2j} - \lambda_j \mathbf{K}_{2j}^{\mathrm{T}} - \left(\lambda_j + 4\mu_j\right) K_{6j} \right] \tag{A5}$$

$$\mathbf{Z}_{2t} = \sum_{j=1}^{m} \left[\mu_j \mathbf{K}_{1j} - \mu_j \mathbf{K}_{2j} + \left(\lambda_j + 2\mu_j\right) n^2 \mathbf{K}_{6j} - 2\mu_j \mathbf{K}_{2j}^{\mathrm{T}} + 2\mu_j \mathbf{K}_{6j} - \rho_j \omega^2 \mathbf{K}_{4j} \right] \tag{A6}$$

$$\mathbf{Z}_{2z} = nk\sum_{j=1}^{m}\left(\lambda_j+\mu_j\right)\mathbf{K}_{5j} \tag{A7}$$

$$\mathbf{Z}_{2s} = -k^2\sum_{j=1}^{m}\mu_j\mathbf{K}_{4j} \tag{A8}$$

$$\mathbf{Z}_{3r} = -ik\sum_{j=1}^{m}\left[\mu_j\mathbf{K}_{3j}^{\mathrm{T}}-\lambda_j\mathbf{K}_{3j}-\left(\lambda_j+\mu_j\right)\mathbf{K}_{5j}\right] \tag{A9}$$

$$\mathbf{Z}_{3t} = nk\sum_{j=1}^{m}\left(\lambda_j+\mu_j\right)\mathbf{K}_{5j} \tag{A10}$$

$$\mathbf{Z}_{3z} = \sum_{j=1}^{m}\left[\mu_j\mathbf{K}_{1j}+n^2\mu_j\mathbf{K}_{6j}-\mu_j\mathbf{K}_{2j}^{\mathrm{T}}-\rho_j\omega^2K_{4j}\right] \tag{A11}$$

$$\mathbf{Z}_{3s} = -k^2\sum_{j=1}^{m}\left(\lambda_j+2\mu_j\right)\mathbf{K}_{4j} \tag{A12}$$

For layers $j=1, m-1$

$$\mathbf{K}_{1j} = \int_{a_j}^{b_j}\frac{\partial\mathbf{N}^{\mathrm{T}}}{\partial r}\frac{\partial\mathbf{N}}{\partial r}dr \tag{A13}$$

$$\mathbf{K}_{2j} = \int_{a_j}^{b_j}\frac{1}{r}\frac{\partial\mathbf{N}^{\mathbf{T}}}{\partial r}\mathbf{N}dr \tag{A14}$$

$$\mathbf{K}_{3j} = \int_{a_j}^{b_j}\mathbf{N}^{\mathbf{T}}\frac{\partial\mathbf{N}}{\partial r}dr \tag{A15}$$

$$\mathbf{K}_{4j} = \int_{a_j}^{b_j}\mathbf{N}^{\mathrm{T}}\mathbf{N}dr \tag{A16}$$

$$\mathbf{K}_{5j} = \int_{a_j}^{b_j}\frac{1}{r}\mathbf{N}^{\mathrm{T}}\mathbf{N}dr \tag{A17}$$

$$\mathbf{K}_{6j} = \int_{a_j}^{b_j}\frac{1}{r^2}\mathbf{N}^{\mathrm{T}}\mathbf{N}dr \tag{A18}$$

For the PML region, $j=m$

$$\mathbf{K}_{1m} = \int_{a_m}^{b_m}\frac{1}{\xi_r}\frac{\partial\mathbf{N}^{\mathrm{T}}}{\partial r}\frac{\partial\mathbf{N}}{\partial r}dr \tag{A19}$$

$$\mathbf{K}_{2m} = \int_{a_m}^{b_m}\frac{1}{r_{\sim}}\frac{\partial\mathbf{N}^{\mathrm{T}}}{\partial r}\mathbf{N}dr \tag{A20}$$

$$\mathbf{K}_{3m} = \int_{a_m}^{b_m}\mathbf{N}^{\mathrm{T}}\frac{\partial\mathbf{N}}{\partial r}dr \tag{A21}$$

$$\mathbf{K}_{4m} = \int_{a_m}^{b_m}\xi_r\mathbf{N}^{\mathrm{T}}\mathbf{N}dr \tag{A22}$$

$$\mathbf{K}_{5m} = \int_{a_m}^{b_m}\frac{\xi_r}{r_{\sim}}\mathbf{N}^{\mathrm{T}}\mathbf{N}dr \tag{A23}$$

$$\mathbf{K}_{6m} = \int_{a_m}^{b_m}\frac{\xi_r}{r_{\sim}^{\,2}}\mathbf{N}^{\mathrm{T}}\mathbf{N}dr \tag{A24}$$

Note that for a buried rod, $a_1=0$, which means that $1/r$ is singular at the centre of the rod; however, for this scenario the governing equations enforce zero normal and shear stresses at the centre and so this singularity is avoided in the usual way.

References

[1] M.J.S. Lowe, D.N. Alleyne, P. Cawley, Defect detection in pipes using guided waves, *Ultrasonics* 36 (1998) 147–154.
[2] W. Duan, R. Kirby, A numerical model for the scattering of elastic waves from a non-axisymmetric defect in a pipe, *Finite Elements in Analysis and Design* 100 (2015) 28–40.
[3] M.J. Brennan, Y. Gao, P.F. Joseph, On the relationship between time and frequency domain methods in time delay estimation for leak detection in water distribution pipes, *Journal of Sound and Vibration* 304 (2007) 213–223.
[4] J.M. Muggleton, J. Yan, Wavenumber prediction and measurement of axisymmetric waves in buried fluid-filled pipes: Inclusion of shear coupling at a lubricated pipe/soil interface, *Journal of Sound and Vibration* 332 (2013) 1216–1230.
[5] R. Kirby, Z. Zlatev, P. Mudge, On the scattering of torsional elastic waves from axisymmetric defects in coated pipes, *Journal of Sound and Vibration* 331 (2012) 3989–4004.
[6] R. Kirby, Z. Zlatev, P. Mudge, On the scattering of longitudinal elastic waves from axisymmetric defects in coated pipes, *Journal of Sound and Vibration* 332 (2013) 5040–5058.
[7] W. Duan, R. Kirby, P. Mudge, On the scattering of elastic waves from a non-axisymmetric defect in a coated pipe, *Ultrasonics* 65 (2016) 228–241.
[8] M.J.S. Lowe, Matrix techniques for modelling ultrasonic waves in multi-layered media, *IEEE Transactions on Ultrasonics Ferroelectrics and Frequency Control* 47 (4) (1995) 525–542.
[9] B. Pavlakovic, M.J.S. Lowe, D. Alleyne, P. Cawley, Disperse: a general purpose program for creating dispersion curves, in: D.O. Thompson, D.E. Chimenti (Eds.), *Review of Progress in Quantitative Nondestructive Evaluation*, Vol. 16A, , Springer, New York1997, pp. 185–192.
[10] R. Long, P. Cawley, M.J.S. Lowe, Acoustic wave propagation in buried iron water pipes, *Proceedings of the Royal Society A: Mathematical, Physical and Engineering Sciences* 459 (2003) 2749–2770.
[11] E. Leinov, M.J.S. Lowe, P. Cawley, Investigation of guided wave propagation and attenuation in pipe buried in sand, *Journal of Sound and Vibration* 347 (2015) 96–114.
[12] E. Leinov, M.J.S. Lowe, P. Cawley, Ultrasonic isolation of buried pipes, *Journal of Sound and Vibration* 363 (2016) 225–239.
[13] R. Kirby, A comparison between analytic and numerical methods for modelling automotive dissipative silencers with mean flow, *Journal of Sound and Vibration* 325 (2009) 565–582.
[14] B. Pavlakovic, M.J.S. Lowe, P. Cawley, High frequency low-loss ultrasonic modes in imbedded bars, *Journal of Applied Mechanics* 68 (2001) 67–75.
[15] J.A. Simmons, E. Drescher-Krasicka, H.N.G. Wadley, Leaky axisymmetric modes in infinite clad rods. I, *Journal of the Acoustical Society of America* 92 (2) (1992) 1061–1090.
[16] F. Treyssède, L. Laguerre, Numerical and analytical calculation of modal excitability for elastic wave generation in lossy waveguides, *Journal of the Acoustical Society of America* 133 (2013) 3827–3837.
[17] A. Marzani, E. Viola, I. Bartoli, F. Lanza di Scalea, P. Rizzo, A semi-analytical finite element formulation for modelling stress wave propagation in axisymmetric damped waveguides, *Journal of Sound and Vibration* 318 (2008) 488–505.
[18] J. Mu, J.L. Rose, Guided wave propagation and mode differentiation in hollow cylinders with viscoelastic coatings, *Journal of the Acoustical Society of America* 124 (2008) 866–874.
[19] M. Castaings, M. Lowe, Finite element model for waves guided along solid systems of arbitrary section coupled to infinite solid media, *Journal of the Acoustical Society of America* 123 (2008) 696–708.
[20] J. Hua, J. Mu, J.L. Rose, Guided wave propagation in single and double layer hollow cylinders embedded in infinite media, *Journal of the Acoustical Society of America* 129 (2011) 691–700.
[21] R.J. Astley, Infinite elements for wave problems: a review of current formulations and an assessment of accuracy, *International Journal for Numerical Methods in Engineering* 49 (2000) 951–976.
[22] H. Gravenkamp, C. Birk, C. Song, Computation of dispersion curves for embedded waveguides using dashpot boundary condition, *Journal of the Acoustical Society of America* 135 (3) (2014) 1127–1138.
[23] H. Gravenkamp, C. Birk, J. Van, Modeling ultrasonic waves in elastic waveguides of arbitrary cross-section embedded in infinite solid medium, *Computers and Structures* 149 (2015) 61–71.
[24] M. Mazzotti, I. Bartoli, A. Marzani, E. Viola, A coupled SAFE-2.5D BEM approach for the dispersion analysis of damped leaky guided waves in embedded waveguides of arbitrary cross-section, *Ultrasonics* 53 (2013) 1227–1241.
[25] J.-P. Berenger, A perfectly matched layer for the absorption of electromagnetic waves, *Journal of Computational Physics* 114 (1994) 185–200.
[26] W.C. Chew, W.H. Weedon, A 3D perfectly matched medium from modified Maxwell's equations with stretched coordinates, *Microwave and Optical Technology Letters* 7 (13) (1994) 599–604.
[27] Q. Qi, T.L. Geers, Evaluation of the perfectly matched layer for computational acoustics, *Journal of Computational Physics* 139 (1998) 166–183.
[28] K.L. Nguyen, F. Treyssède, C. Hazard, Numerical modeling of three-dimensional open elastic waveguides combining semi-analytical finite element and perfectly matched layer methods, *Journal of Sound and Vibration* 344 (2015) 158–178.
[29] B.A. Auld, *Acoustics Fields and Waves in Solids*, Krieger, Malabar FL, 1990.
[30] W.C. Chew, Q.H. Liu, Perfectly matched layers for elastodynamics: a new absorbing boundary condition, *Journal of Computational Acoustics* 4 (1996) 341–359.
[31] M. Silk, K. Bainton, The propagation in metal tubing of ultrasonic wave modes equivalent to Lamb waves, *Ultrasonics* 17 (1979) 11–19.
[32] R. Cimpeanu, A. Martinsson, M. Heil, A parameter-free perfectly matched layer formulation for the finite-element-based solution of the Helmholtz equation, *Journal of Computational Physics* 296 (2015) 329–347.
[33] C. Michler, L. Demkowicz, J. Kurtz, D. Pardo, Improving the performance of perfectly matched layers by means of *hp*-adaptivity, *Numerical Methods for Partial Differential Equations* 23 (2007) 832–858.
[34] D. Rabinovich, D. Givoli, E. B´ecache, Comparison of high-order absorbing boundary conditions and perfectly matched layers in the frequency domain, *International Journal for Numerical Methods in Biomedical Engineering* 26 (2010) 1351–1369.
[35] A. Fathi, B. Poursartip, L.F. Kallivokas, Time-domain hybrid formulations for wave simulations in three-dimensional PML-truncated heterogeneous media, *International Journal for Numerical Methods in Engineering* 101 (2015) 165–198.
[36] I. Singer, E. Turkel, A perfectly matched layer for the Helmholtz equation in a semi-infinite strip, *Journal of Computational Physics* 201 (2004) 439–465.
[37] N. Barshinger, J.L. Rose, Guided wave propagation in an elastic hollow cylinder coated with a viscoelastic material, *IEEE Transactions on Ultrasonics, Ferroelectrics, and Frequency Control* 51 (2004) 1547–1556.